NEUROSCIENCE

Julich-Brain: A 3D probabilistic atlas of the human brain's cytoarchitecture

Katrin Amunts[1,2]*†, Hartmut Mohlberg[1]*†, Sebastian Bludau[1], Karl Zilles[1]

Cytoarchitecture is a basic principle of microstructural brain parcellation. We introduce Julich-Brain, a three-dimensional atlas containing cytoarchitectonic maps of cortical areas and subcortical nuclei. The atlas is probabilistic, which enables it to account for variations between individual brains. Building such an atlas was highly data- and labor-intensive and required the development of nested, interdependent workflows for detecting borders between brain areas, data processing, provenance tracking, and flexible execution of processing chains to handle large amounts of data at different spatial scales. Full cortical coverage was achieved by the inclusion of gap maps to complement cortical maps. The atlas is dynamic and will be adapted as mapping progresses; it is openly available to support neuroimaging studies as well as modeling and simulation; and it is interoperable, enabling connection to other atlases and resources.

Maps of the microstructural segregation of the human brain can offer improved understanding of the biological substrates of brain functions, dysfunctions, and behavior. Cytoarchitecture—the arrangement of cells, their distribution, composition, and layering—is a major principle of microstructural brain organization. It is closely linked to the connectivity pattern of a region and its function (*1*). Furthermore, cytoarchitecture allows multiple aspects of brain organization (such as myeloarchitecture, molecular architecture, gene expression, and activation or resting-state networks) to be referenced to a common ground that serves as the interface to represent and integrate the different aspects of brain organization (*2*). It is widely accepted that a multifaceted but integrated approach is a prerequisite for research into brain organization (*3*, *4*).

Brodmann's cytoarchitectonic map from 1909 was one of the first maps of its kind and is still widely used. It has several limitations; for example, it shows only the left hemisphere of a single brain and therefore cannot account for intersubject variability. Evidence has been obtained that the number of cortical areas is in the range of 180 or more (*2*, *5*, *6*), as compared to 43 areas in Brodmann's map. Subcortical structures have been mapped with the same level of detail (*7*) but are not part of the Brodmann atlas. Without analyzing and processing thousands of histological sections per brain with consistently high quality, the variable cytoarchitecture of areas and nuclei in a cytoarchitectonic map cannot be captured with sufficient spatial resolution (*8*).

[1]Institute of Neuroscience and Medicine (INM-1), Research Centre Jülich, Jülich, Germany. [2]C. and O. Vogt Institute for Brain Research, University Hospital Düsseldorf, Heinrich Heine University Düsseldorf, Düsseldorf, Germany.
*Corresponding author. Email: k.amunts@fz-juelich.de (K.A.); h.mohlberg@fz-juelich.de (H.M.)
†These authors contributed equally to this work.

We created the Julich-Brain atlas in our labs in Jülich and Düsseldorf (Fig. 1). It is a cytoarchitectonic atlas containing probabilistic maps of cortical areas and subcortical nuclei. Having started this endeavor in the mid-1990s, we more recently resorted to "crowdsourcing" strategies (but on a high professional level and based on profound expertise), which in turn required Big Data–capable processing workflows. All of the necessary steps—preparation of human brain tissue, microstructural mapping, analysis, and complex data processing—are data-, time-, and labor-intensive, all the more so with increasing sample sizes and higher spatial resolution. It is thus impossible to provide whole-brain maps with sufficient detail by single researchers or small teams in an acceptable time frame. Increased computing power and storage capacities, as well as improved algorithms and workflows for data processing, now enable much faster and more robust processing at high spatial resolution.

However, not all datasets and analyses benefit equally from improved data acquisition techniques. Our cytoarchitectonic mapping efforts started more than 25 years ago. The brains have already been histologically processed, and neither new high-field magnetic resonance imaging (MRI) data nor high-resolution blockface images can be acquired afterward. The quality of MRI data is thus constrained by the quality available at the time of acquisition. This may sometimes restrict the use of modern imaging tools and techniques, because these are often geared toward currently available data quality. Specific data processing strategies considering both recent and older datasets are mandatory. To ensure accuracy, reproducibility, and consistency of data and processing steps over the entire data life cycle, automated and reproducible workflows governed by provenance tracking are necessary.

We therefore developed a modular, flexible, and adaptive framework to create probabilistic cytoarchitectonic maps, resulting from the analysis of 10 postmortem human brains, for each area (Fig. 2). Maps were aligned to two widely used stereotaxic spaces, MNI-Colin27 and ICBM152casym space (*9*), and superimposed. The Julich-Brain atlas allows comparison of functional activations, networks, genetic expression patterns, anatomical structures, and other data obtained across different studies in a common stereotaxic reference space (Fig. 3). The framework relies on longstanding expertise for handling whole human postmortem brains, cytoarchitectonic mapping of a variety of cortical and subcortical regions, and computational expertise to develop robust and adaptive tools, using both local clusters and supercomputers. All of these aspects have changed over time, and the creation of a uniform, reproducible, and probabilistic brain atlas depends on their convergence.

The Julich-Brain atlas is based on histological sections of 23 postmortem brains (11 female, 12 male; mean age = 64 years, age range = 30 to 86 years; mean postmortem delay = 12 hours; table S1) acquired from the body donor programs of the Anatomical Institute of the University of Düsseldorf. The brains were fixed in formalin or Bodian solution, subjected to MRI, embedded in paraffin, and serially cut with a microtome into 20-μm sections (*10*). Cell bodies were stained using a modified Merker method. Histological sections were digitized with flatbed scanners at 10 μm, reduced to an isotropic resolution of 20 μm, framed to a fixed picture size, and stored as lossless compressed gray-level images. Two brains constitute complete series [the "BigBrain datasets," one of which was published in (*11*)], where every single section was stained and digitized. The other brains were stained with intervals of up to 15 sections. This resulted in more than 24,000 histological sections. Histological processing and staining, including mounting of sections and removal of small wrinkles and folds, entailed some degree of local deformation, damage, or staining inhomogeneity. Although this was unavoidable, fewer than 1% of the sections showed irretrievable damage (e.g., loss of substantial parts of the tissue), and 20 to 30% had small, local damages. To correct for distortions in histological sections, we used the corresponding MRI datasets for 3D reconstruction (Fig. 2). Rather severe areas of damage in images of histological sections were manually and, where applicable, semiautomatically corrected (*11*) (fig. S1A).

The time-consuming repairs and the considerable amount of computing time for processing the BigBrain datasets required a workflow using supercomputers. The large number of

datasets, in combination with the complexity and diversity of the overall reconstruction workflow, required time- and resource-effective computational processing. This in turn required advanced management of big datasets, computing, and provenance tracking (fig. S1). On the basis of the reconstruction of BigBrain 1 (*11*), an adapted workflow was developed for the reconstruction of BigBrain 2, which includes an elaborate data provenance tracking system. It served as the basis for a general-purpose dataflow management system that allowed restricting the recalculation to only those images that were affected by subsequent repairs (fig. S1A), resulting in a substantial reduction of computing time (*12*). In addition, the pipeline of the BigBrain 2 dataset was closely linked to the overall workflow and was used in a similar way as for the other 21 postmortem brains. To recover the original shape and topology of the brain volume, we computed a 3D reconstruction of histological sections (fig. S3); for a recent survey of methods, see (*13*). The approach is based on a multistep procedure starting from an initially 3D dataset at a resolution of 0.3 mm^3 and is explained in the supplementary materials.

Human brains show a variable pattern of sulci and gyri, plus intersubject variability in shape, localization, and extent of cytoarchitectonic regions (*2*). To make brains comparable, we initially transferred 3D reconstructed histological datasets to the stereotaxic space of the single-subject MNI-Colin27 template (fig. S3). In contrast to templates resulting from an "average" of many brain datasets [e.g., the MNI305 template (*9*)], the individual reference brain shows a detailed (but not representative) anatomy, thus allowing a precise registration of the gross anatomy of the postmortem brains to that space. Because mean group datasets are well accepted in the neuroimaging community, nonlinear transformations into the ICBM2009casym space were also computed. This template represents a compromise between the detailed but specific anatomy of the MNI-Colin27 brain and the more generic but smoother MNI305 template. The representation of the maps in these two spaces makes Julich-Brain interoperable with other atlases and resources [e.g., (*6*, *7*, *14*, *15*)] and connects it to large cohort studies such as the Human Connectome Project (HCP; www.humanconnectome.org) and UK Biobank (www.ukbiobank.ac.uk) (see also supplementary materials).

Different approaches are available to register postmortem brains to each other [for an overview, see (*13*)]. To develop an atlas with both cortical areas and subcortical nuclei, we started with a volume-based approach, which provided a consistent registration framework for both cortical and subcortical structures. An elastic 3D registration was applied with a well-matched parameter set that was also used for the 2D registrations. The method showed high reliability in both postmortem and in vivo datasets. The registration of all postmortem brains to the MNI-Colin27 and the ICBM152casym reference brains resulted in a similar folding pattern and shape of the 3D-reconstructed datasets and the template (fig. S3). The 3D vector field transformations of each 3D-reconstructed histological dataset were stored and were later applied to the mapped cytoarchitectonic areas.

To date, 41 projects have resulted in maps of 248 cytoarchitectonic areas (Fig. 1). Projects were carried out by doctoral students, researchers, and guest scientists and have been published in peer-reviewed scientific journals [for an overview, see (*2*)]. These publications provide details of cytoarchitecture, localization with respect to sulci/gyri and stereotaxic space, intersubject variability, and other features; some of them also refer to the relationship of the areas to functional imaging studies, receptor architecture, and/or area-specific gene expression.

Each map is based on analyses of 10 postmortem brains (5 male, 5 female), which were selected from the pool of 23 brains on the basis of their folding pattern, the presence of already mapped neighboring areas, the orientation of the cutting plane, etc. Consequently, overlapping and sometimes similar samples were analyzed for different regions.

Depending on the size and shape of a structure, every 15th to 60th section was mapped over the whole extent of a cytoarchitectonic region. Borders between cortical areas were identified using image analysis and statistical criteria to make mapping reproducible (*16*). The positions of borders were labeled in the digitized sections, and a closed polygon (contour line) marked its extent in the section (fig. S4). For subcortical nuclei, the outer boundaries of nuclei were identified in histological sections and labeled as closed polygonal lines. Contour lines were also used for a quality check of each map over its full extent (fig. S4).

As a next step, individual shrinkage-corrected volumes for each area/nucleus, hemisphere, and brain were calculated (see supplementary materials). The analysis of the 120 currently available areas showed considerable

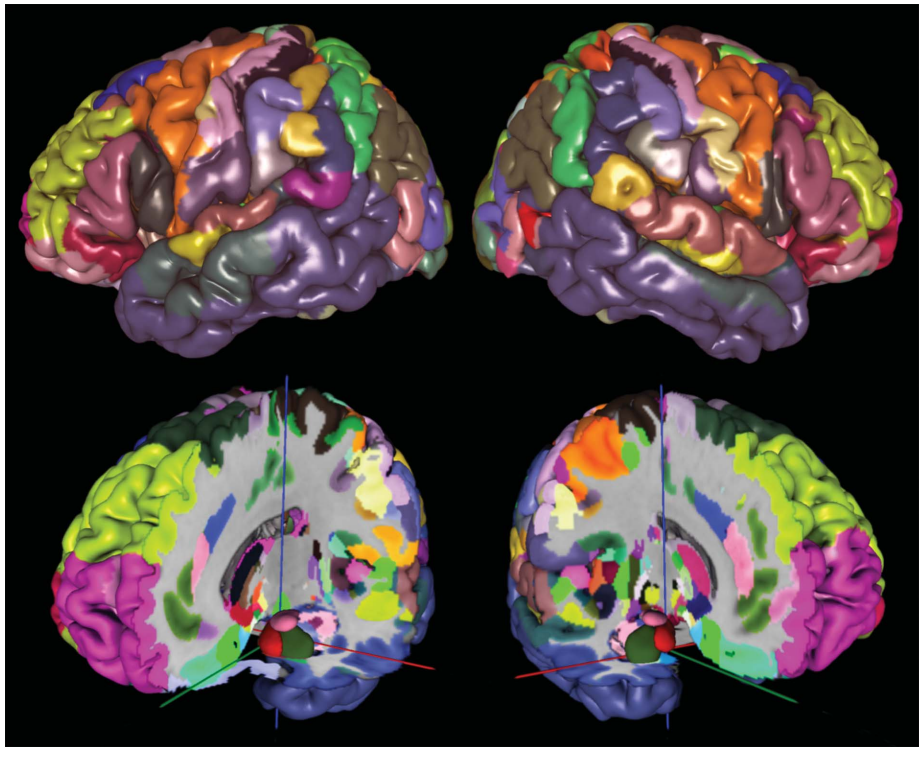

Fig. 1. Cytoarchitectonic maximum probability maps of Julich-Brain in MNI-Colin27 reference space. Areas have different colors; views of the left and right hemispheres are shown. The lower panel shows structures located in the depths of the brain. Datasets of published areas are freely available through the Julich-Brain and HBP data portals. Both web-based interfaces allow the visualization and inspection of probabilistic and maximum probability maps as surface (pial, smoothed white matter, inflated) and volume representations.

intersubject differences in volume (fig. S5), but differences between the two hemispheres were not significant at a global level, nor were differences between male and female brains (see table S2 for full information on these volumes). The list of volumes is a growing resource together with the probabilistic maps of areas and nuclei, made available and constantly updated through the Knowledge graph of the European Human Brain Project (HBP; see https://ebrains.eu).

The comparison of the degree of intersubject variability suggests differences between brain regions (fig. S5). For example, we found high variability (i.e., low values for probability) in Broca's region with areas 44 and 45 and the superior parietal lobule, whereas the occipital pole with the primary and secondary visual cortices (BA17/18) and area Te3 in the temporal lobe appeared less variable.

Previous and ongoing mapping projects resulted in more than 10,616 XML files containing 85,210 contour lines with 3,737,771 points and a total length of 1961 m. Stacks with contour lines were managed using the open-source version control software Subversion, which automatically manages files and directories so as to document the complete history of how the localization of an areal border might have changed over its life cycle (fig. S1B). Changes may occur when a new mapping project requires reanalysis of an already existing map, but these have been small in the past.

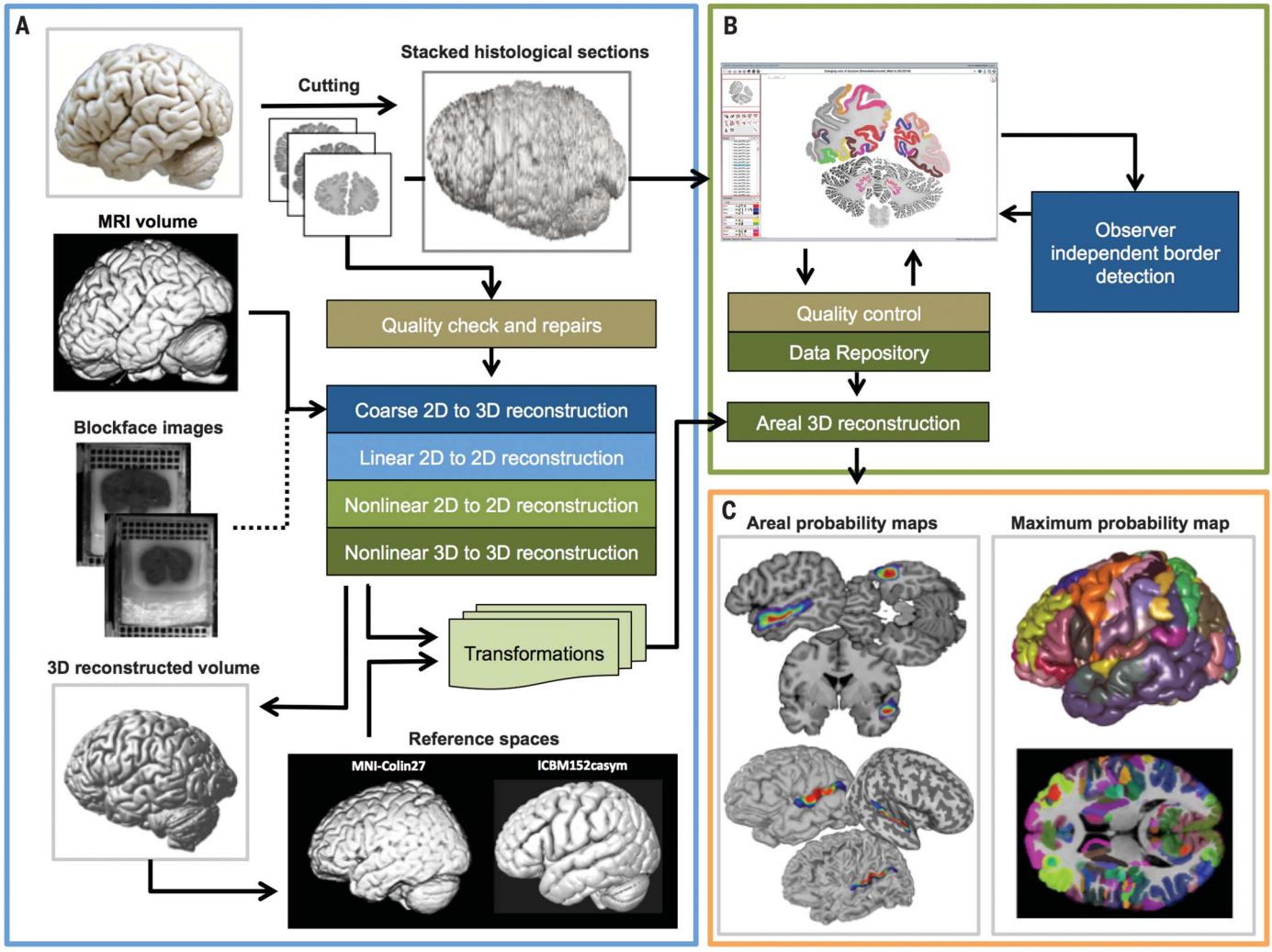

Fig. 2. Workflow of the 3D reconstruction of serial histological sections and alignment of brain data to a reference space, cytoarchitectonic analysis in 2D images, and the computing of the probabilistic Julich-Brain atlas. (**A**) To recover the 3D shape of a postmortem brain, we applied a combination of linear and nonlinear processing steps at different scales based on the undistorted MRI dataset, and optional on blockface images, obtained during sectioning. The digitized histological images were repaired and corrected for illumination and optical imbalances. A rigid section-to-section alignment was computed to create a first approximate 3D reconstruction. It served to align the MRI dataset to the corresponding section planes by a rigid-body transformation. The sections were nonlinearly registered to the sections of the MRI by an elastic method. The alignment was improved by re-registering the output several times, section by section, to a median filtered version. (**B**) The cytoarchitecture was analyzed in consecutive histological sections covering the complete extent of an area and characterized by the gray-level index (*16*). Contour lines of the areas were submitted to a data repository, 3D-reconstructed, and topologically normalized. Linear and nonlinear transformations were applied to the areas, and areas were superimposed to form the cytoarchitectonic probability map. (**C**) Volume- and surface-based maximum probability maps of the Julich-Brain atlas were computed. To effectively organize the intensive computations, we implemented a data processing management system that allowed distributed processing of a large number of datasets across multiple CPU cores. It was designed to scale up well from a single core computer system up to thousands of computing nodes in a high-performance computing environment (*12*). See fig. S1, A to C, for details.

The areas and nuclei were also transformed to the stereotaxic MNI-Colin27 and ICBM2009casym reference space, using the computed whole-brain transformations, and superimposed (see supplementary materials). The resulting probabilistic, cytoarchitectonic maps were stored as volume data files. By projecting the probability values onto the surface, a surface-based representation of cytoarchitectonic cortical maps was computed (Fig. 1 and fig. S6). The resulting values, indicating the probability of an area or nucleus being localized in a given voxel (0% to 100% overlap), range from 0.0 to 1.0; this number provides a measure for variations of a given area in localization and extent from brain to brain (i.e., intersubject variability). These probabilistic maps overlap with each other; that is, voxels in reference space can usually be assigned to more than one area, each with a well-defined probability, summing up to 100% (fig. S6). We found that about 50% of the voxels were associated with a single area or nucleus, 35% with two, and 15% with three or more.

To reduce complexity and to visualize the extent of areas comparable to Brodmann's map, we calculated a maximum probability map (MPM). Each voxel in the reference brain was assigned to the cytoarchitectonic area with the highest probability at that position (*17*). The average overlap fraction of all currently

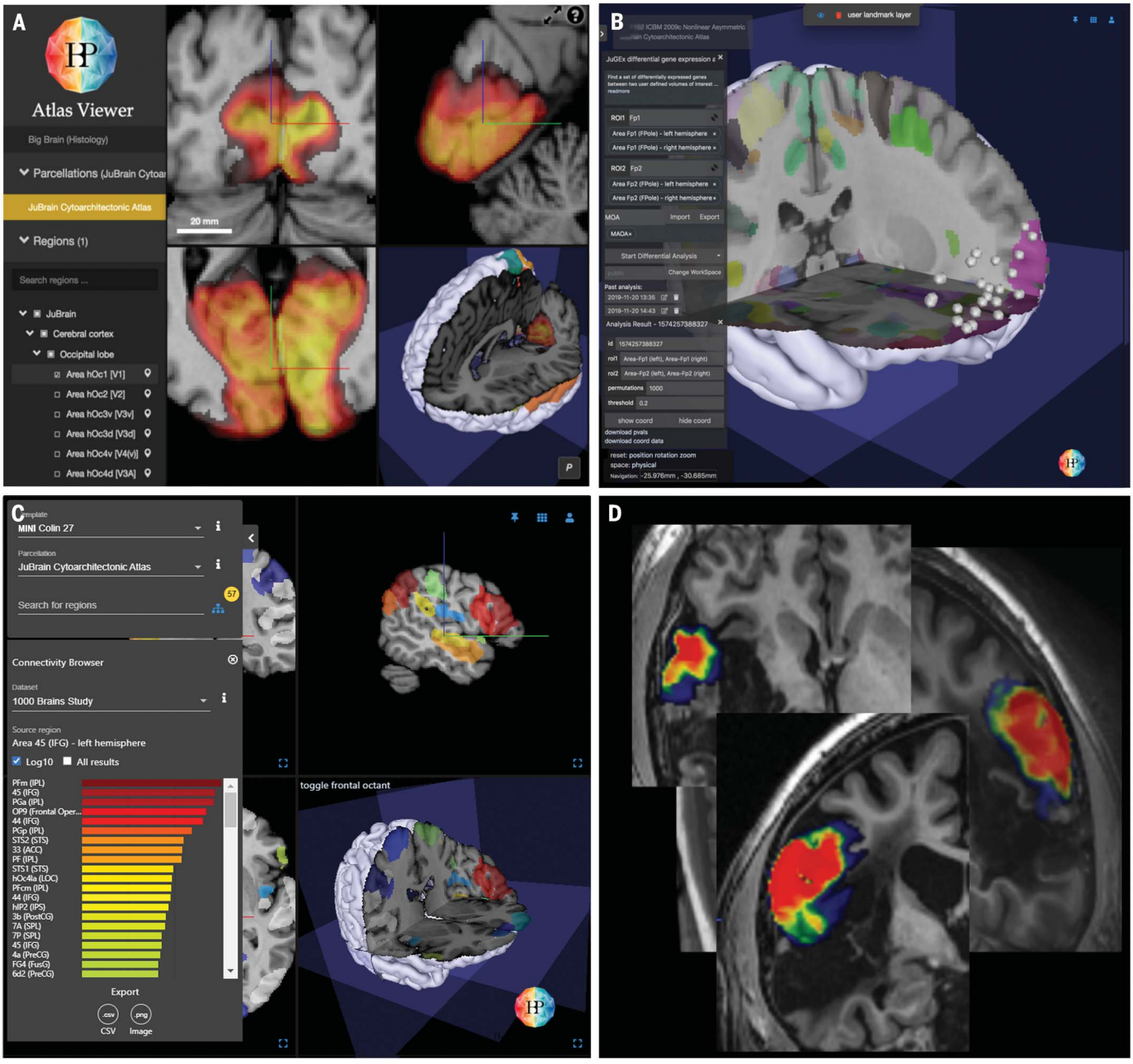

Fig. 3. Examples of applications of the Julich-Brain atlas. (**A**) Screenshot of the web-based atlas tool in the Human Brain Atlas of the HBP showing probability maps in different views. (**B** and **C**) JuGEx enables analysis of differential gene expression in cytoarchitectonic maps (B) and linkage and exploration of DTI-based connectivity (e.g., left Broca's area 45) (C). (**D**) Superposition of the probabilistic map of Broca's area 44 on a dataset of a patient with a brain lesion and aphasia. The maps allow precise statements about the microanatomical location of a neuroimaging finding, and are a tool to quantify these findings by using the maps as a mask.

mapped and adjacent areas results in a threshold value of about 35%. Under the assumption that this threshold also applies to MPM borders to yet unmapped areas, this threshold is used to cut the MPM toward unmapped regions. The visualization of neighboring areas demonstrates that gyri may be occupied by one or more areas that differ in cytoarchitecture and function. Conversely, single areas may be found on more than one gyrus; examples are given for the auditory cortex in fig. S7. The manifold of relationships between areas and sulci/gyri illustrates the advantage and higher precision of cytoarchitectonic probabilistic maps as compared to macroscopic brain maps.

At present, about 70% of the cortical surface has been covered by completed and published mapping projects. However, there are still areas that have not been mapped and represent projects for future research. To provide whole-brain coverage for the cortex (fig. S8), we have combined parts of the cortex that have not yet been charted into several "gap maps," pooling these uncharted areas in a given brain region (see supplementary materials and fig. S9). The distributions were modeled so that probabilistic gap maps were computed in analogy to the other maps. As mapping progresses, new maps are continuously replacing gap maps while the process is captured and documented by provenance tracking. Consequently, the atlas is not static (as is, e.g., Brodmann's map) but rather represents a "living map"—a concept that is known, for example, from geography for navigating complex spaces.

Gap maps allow computation of a parcellation covering the entire cortical surface and the unambiguous assignment of each position to a cortical region. Together with the increasing number of probabilistic maps of subcortical nuclei, gap maps contribute to a whole-brain human atlas. Maps in Julich-Brain can be combined with findings in other atlases and maps; one example involves the study of microstructural correlates of activations from neuroimaging studies of healthy subjects and patients (Fig. 3). Moreover, Julich-Brain contributes to brain modeling and simulation through informing the model by a functionally sound microstructural parcellation. It is expected that this will open new avenues to generate models of brain activity such as those used in the treatment of epilepsy, where personalized brain models are used to predict the propagation of seizures (*18*).

The modular, flexible, and extensible workflows cover a broad range of steps from image acquisition to 3D reconstruction and the generation of probabilistic maps, which can be found in several areas of research. The methodical framework (or parts of it) can be extended to brains of other species, and it can be used to process section images labeled by other techniques (e.g., immunohistology). New modules can be added to the workflows for applications such as mapping brain areas on the basis of deep learning (*19*).

The Julich-Brain atlas is a freely available resource (www.julich-brain.org). Maps have been made available through different tools and websites such as the SPM anatomy toolbox (www.fz-juelich.de/inm/inm-7/JuelichAnatomyToolbox), FSL (https://fsl.fmrib.ox.ac.uk), FreeSurfer (https://surfer.nmr.mgh.harvard.edu), and the EBRAINS research infrastructure of the HBP (https://ebrains.eu/services/atlases). The maps can be linked to diffusion tensor imaging (DTI)–based connectivity data (Fig. 3C) and to gene expression data provided by the Allen Institute for Brain Science (https://alleninstitute.org/what-we-do/brain-science) through the JuGEx tool (*20*) to enable a multimodal perspective on human brain organization (Fig. 3B).

Julich-Brain represents a new kind of human brain atlas that is (i) cytoarchitectonic to reflect a basic principle of the brain's microstructural parcellation; (ii) whole-brain,to cover both the cerebral cortex and subcortical nuclei; (iii) 3D-probabilistic, to consider variations between individual brains in stereotaxic space; (iv) dynamic, a living atlas, to be supplemented by maps of new areas or subdivision of existing maps of areas (e.g., when new studies suggest a finer or new parcellation); (v) flexible, to allow for modifications of modules in the workflows for other data modalities, organs, or species; (vi) open-access and based on FAIR principles, to contribute to studies by other researchers addressing structure-function relationships and network organization; and (vi) interoperable, to link it to other atlases and resources that provide complementary information about brain organization.

REFERENCES AND NOTES

1. A. Goulas, K. Zilles, C. C. Hilgetag, *Trends Neurosci.* **41**, 775–788 (2018).
2. K. Amunts, K. Zilles, *Neuron* **88**, 1086–1107 (2015).
3. D. C. Van Essen *et al*., *Proc. Natl. Acad. Sci. U.S.A.* **116**, 26173–26180 (2019).
4. B. Fischl, M. I. Sereno, *Neuroimage* **182**, 219–231 (2018).
5. R. Nieuwenhuys, C. A. J. Broere, *Brain Struct. Funct.* **222**, 465–480 (2016).
6. M. F. Glasser *et al*., *Nature* **536**, 171–178 (2016).
7. J. K. Mai *et al*., *Atlas of the Human Brain* (Academic Press, ed. 4, 2015).
8. K. Zilles, K. Amunts, *Nat. Rev. Neurosci.* **11**, 139–145 (2010).
9. A. C. Evans, A. L. Janke, D. L. Collins, S. Baillet, *Neuroimage* **62**, 911–922 (2012).
10. K. Amunts *et al*., *J. Neurosci.* **27**, 1356–1364 (2007).
11. K. Amunts *et al*., *Science* **340**, 1472–1475 (2013).
12. H. Mohlberg *et al*., in *Brain-Inspired Computing: Second International Workshop, BrainComp 2015*, K. Amunts *et al*., Eds. (Springer, 2016), pp. 15–27.
13. J. Pichat, J. E. Iglesias, T. Yousry, S. Ourselin, M. Modat, *Med. Image Anal.* **46**, 73–105 (2018).
14. H. Damasio, *Human Brain Anatomy in Computerized Images* (Oxford Univ. Press, ed. 2, 2005).
15. S. L. Ding *et al*., *J. Comp. Neurol.* **524**, 3127–3481 (2016).
16. A. Schleicher *et al*., *Anat. Embryol.* **210**, 373–386 (2005).
17. S. B. Eickhoff *et al*., *Neuroimage* **25**, 1325–1335 (2005).
18. T. Proix, F. Bartolomei, M. Guye, V. K. Jirsa, *Brain* **140**, 641–654 (2017).
19. H. Spitzer *et al*., in *Medical Image Computing and Computer Assisted Intervention—MICCAI 2018, Part III*, A. F. Frangi *et al*., Eds. (Springer, 2018), pp. 663–671.
20. S. Bludau *et al*., *Brain Struct. Funct.* **223**, 2335–2342 (2018).

ACKNOWLEDGMENTS

We thank more than 41 postdocs, doctoral students, guests, and colleagues who contributed to the mapping of 248 cytoarchitectonic areas and nuclei; the technical assistants of the C. and O. Vogt Institute of Heinrich Heine University Düsseldorf and Research Centre Jülich; S. Eickhoff, R. Hübbers, P. Pieperhoff, N. Palomero-Gallagher, S. Caspers, T. Dickscheid, and A. C. Evans for intensive discussions; A. Schleicher for developing the original observer-independent mapping approach; our partners of the International Consortium for Human Brain Mapping who stimulated and actively supported this research; and our colleagues at the Jülich Supercomputing Centre, in particular B. Tweddell and T. Lippert. **Funding:** Supported by the Portfolio Theme "Supercomputing and Modeling for the Human Brain" of the Helmholtz Association, the European Union Seventh Framework Programme (FP7/2007-2013, HBP), and the European Union's Horizon 2020 Research and Innovation Programme, grant agreements 604102 (HBP SGA1), 785907 (HBP SGA2), and 945539 (HBP SGA3). **Author contributions:** K.A. and K.Z. developed the concept of 3D probabilistic cytoarchitectonic brain mapping and atlas. K.A. is overseeing the atlas projects, contributed to methodological developments, and drafted the manuscript. H.M. developed and adapted the methodology and the software for data processing and atlas building, and drafted the manuscript. S.B. developed new tools for analysis and mapping of cytoarchitectonic areas. All authors contributed to the writing of the manuscript. **Competing interests:** The authors declare no competing interests. **Data and materials availability:** All data are available in the main text or the supplementary materials. Various data modalities of the already published maps of brain areas and the complete atlas are available online at www.julich-brain.org and via EBRAINS (https://ebrains.eu/) (DOI: 10.25493/TAKY-64D). Previously developed parts of the workflows were published earlier; new scripts for computing the Julich-Brain Atlas and for analyzing contour lines and gap maps (https://doi.org/10.5281/zenodo.3906413) are provided via the git repository, https://github.com/JulichBrainAtlas.

SUPPLEMENTARY MATERIALS

science.sciencemag.org/content/369/6506/988/suppl/DC1
Materials and Methods
Figs. S1 to S9
Tables S1 and S2
References (*21*–*56*)

27 February 2020; accepted 24 June 2020
Published online 30 July 2020
10.1126/science.abb4588